European Journal of Neuroscience, Vol. 12, pp. 945–954, 2000

Alterations in Purkinje cell spines of calbindin D-28 k and parvalbumin knock-out mice

Marco Vecellio,[1] Beat Schwaller,[1] Michael Meyer,[2] Willi Hunziker,[3] and Marco R. Celio[1]
[1]Institute of Histology and General Embryology, University of Fribourg, CH-1705 Fribourg, Switzerland
[2]Max Planck Institute of Neurobiology, Department of Neurobiochemistry, D-82152 Martinsried, Germany
[3]Roche Vitamins Division, Hoffmann-LaRoche Ltd, 4070 Basel, Switzerland

Keywords: ataxia, calcium-binding protein, confocal laser scanning microscopy, 3-D reconstruction, synaptic plasticity

Abstract

The second messenger Ca^{2+} is known to act in a broad spectrum of fundamental cell processes, including modifications of cell shape and motility, through the intermediary of intracellular calcium-binding proteins. The possible impact of the lack of the intracellular soluble Ca^{2+}-binding proteins parvalbumin (PV) and calbindin D-28 k (CB) was tested on spine morphology and topology in Purkinje cell dendrites of genetically modified mice. Three different genotypes were studied, i.e. PV or CB single knock-out ($PV^{-/-}$, $CB^{-/-}$) and PV and CB double knock-out mice ($PV^{-/-}CB^{-/-}$). Purkinje cells were microinjected with Lucifer Yellow and terminal dendrites scanned at high resolution with a confocal laser microscope followed by three-dimensional (3-D) reconstruction. The absence of PV had no significant effect on spine morphology, whereas the absence of CB resulted in a slight increase of various spine parameters, most notably spine length. In double knock-out mice, the absence of both PV and CB entailed a doubling of spine length, an increase in spine volume and spine surface, a higher spine density along the dendrites, as well as a more clustered spine distribution. In all three genotypes, a reduction in the number of stubby spines was observed compared with wild-type animals. These results suggest a morphological compensation for the lack of the soluble calcium buffers in the cytoplasm of Purkinje cell dendritic spines. The increase in various spine parameters, particularly volume, may counteract the lack of the calcium buffers, such as to adjust Ca^{2+}-transients at the transitional zone between spines and dendrites.

Introduction

The second messenger Ca^{2+} is known to act on a broad spectrum of fundamental cell processes, e.g. cell cycle progression (Rasmussen & Means, 1989), cell shape during differentiation (Hennings *et al*., 1980) and cell motility (Marks & Maxfield, 1990). Ca^{2+} signalling is thought to be mediated by cytosolic Ca^{2+}-binding proteins (CaBPs) (Carafoli, 1987), of which parvalbumin (PV) and calbindin D-28 k (CB) are some of the best characterized high-affinity Ca^{2+}-binding proteins of the EF-hand type (Heizmann, 1984). In the nervous system, PV and CB are known as excellent markers for neuronal subpopulations and in the cerebellum they both occur in Purkinje cells (Celio, 1990; Andressen *et al*., 1993). The physiological function of CB and PV in nervous tissue still remains an enigma. They may represent pure Ca^{2+} buffers limiting the amplitude and enhancing the rate of intracellular calcium ($[Ca^{2+}]_i$) decay after Ca^{2+} transients to efficiently reduce $[Ca^{2+}]_i$ below toxic levels, or they may have a Ca^{2+}-dependent regulatory function analogous to that of calmodulin (Heizmann & Braun, 1992). In mice carrying a targeted null mutation of the calbindin D-28 k gene, altered dendritic calcium signalling has been demonstrated (Airaksinen *et al*., 1997). Injection of CB and PV into rat sensory neurons caused a decrease in the rate of the increase in $[Ca^{2+}]_i$ and a faster decay (Chard *et al*., 1993). While no morphological differences in CB-overexpressing cells have been reported, ectopic expression of PV in a ovarian adenocarcinoma cell line (OvGe) led to an increase in the motility of whole cell clusters and a remarkable change in the morphology of the cells from epitheloid to fusiform (Andressen *et al*., 1995).

In view of the influence of CB and PV on Ca^{2+} signalling and cell shape, we decided to investigate Purkinje cell dendritic spine morphology using genetically engineered mice lacking one, or both, of these Ca^{2+}-binding proteins. Dendritic spines are subcompartments of nerve cells which serve as basic functional units of neuronal integration (Yuste & Denk, 1995). The Ca^{2+}-handling properties of spines, i.e. attenuation and propagation of Ca^{2+}-signals, seem to be strongly related to their inherent morphology which can vary considerably (Koch & Zador, 1993). Experimental evidence for spines as modulators of chemical signalling has recently been provided by characterization of the diffusional and electrotonic coupling of spines to dendrites (Svoboda *et al*., 1996). We therefore hypothesized that the absence of Ca^{2+}-binding proteins which would normally reduce the amplitude of Ca^{2+}transients and accelerate the decay of $[Ca^{2+}]_i$ might have an influence on spine morphology.

To test this hypotheses we injected single Purkinje cells with Lucifer Yellow in appropriately fixed tissue slices and applied high-resolution confocal laser scanning microscopy (CLSM) and accurate computer-assisted 3-D reconstruction of terminal branchlets studded with spines to analyse quantitatively these subcompartments in a statistically representative manner. The differences of dendritic structure observed in the CB-lacking mice, and particularly in double-knock out mice, are indicative of a morphological compensation consisting of an increase of spine volume and length. Furthermore, an important role for both proteins during spine

Correspondence: Dr B. Schwaller, as above.
E-mail: Beat.Schwaller @unifr.ch

Received 2 September 1999, revised 1 December 1999, accepted 6 December 1999

morphogenesis is inferred, as their absence results in subtle distribution imbalances of spines which might affect the fine-tuning capability of the Purkinje cell and finally lead to ataxia, as previously observed in CB-deficient mice (Airaksinen *et al.*, 1997).

Materials and methods

Mice

Parvalbumin-deficient ($PV^{-/-}$; Schwaller *et al.*, 1999) and calbindin D-28 k-deficient ($CB^{-/-}$) mice (Airaksinen *et al.*, 1997), generated on a mixed Sv129 × C57Bl/6 genetic background, were used to breed double knock-out mice ($PV^{-/-}CB^{-/-}$). The ratio of double knock-out and wild-type mice was approximately one in 16, as expected from a Mendelian transmission of autosomal genes. All animals were genotyped by polymerase chain reaction and the genotype of all mice was masked until data had been evaluated.

Tissue preparation and Lucifer Yellow injection

Adult male and female $PV^{-/-}$ mice ($n = 6$), $CB^{-/-}$ mice ($n = 5$), $PV^{-/-}CB^{-/-}$ double knock-out mice ($n = 6$), as well as wild-type mice ($n = 5$) were used in the study. The animals (between postnatal day 78 and 204) were deeply anaesthetized by intraperitoneal injection of 4% chloralhydrate (0.1 mL/100 g body weight) and CO_2 for 1 min. The animals were then immediately perfused via the ascending aorta, initially with phosphate buffer (PB) at 4 °C for 30 s and subsequently with 4% (w/v) paraformaldehyde (in 0.1 M PB, pH 7.3) for 5–10 min. All reagents were purchased from Sigma (Buchs, Switzerland) unless indicated otherwise. The brains were removed and placed in cold PB. Parasagittal sections of the cerebella (200 µm thick) were prepared using a vibratome. Sections were immersed overnight in phosphate-buffered saline (PBS) containing 0.04% (w/v) $NaBH_4$, and then rinsed with normal buffer. The Lucifer Yellow injections were performed on the lightly fixed vibratome slices as described previously (Belichenko, 1991), slightly modified from the procedures described by Buhl & Schlote (1987). Fixation was used to reduce the dye leakage previously observed at longer time periods after Lucifer Yellow injection in unfixed cells (Weruaga-Prieto *et al.*, 1996). The only disadvantage of this approach was a slightly enhanced background fluorescence signal, which could be eliminated by applying adequate software-filters during scanning and recalibrating the background base-signal.

In short, a vibratome slice was floated onto a glass plate, and held in place by a filter (Millipore SA, Lausanne, Switzerland) with a window cut slightly smaller in diameter than the area of the underlying tissue. The preparation was placed in a Petri dish and immersed in PB and then transferred to a Zeiss Axioscope fluorescence microscope mounted with a micromanipulator (Zeiss AG, Zurich, Switzerland). Glass microelectrodes (GC 200-F, Clark Electromedical Instruments, Reading, UK) were pulled with a Sutter Instrument (Model P-87, Novato, CA) to an outer tip diameter of 0.3 µm, and were backfilled with a 5% aqueous solution of Lucifer Yellow lithium salt. The vibratome sections were examined using epifluorescence illumination with a fluorescein filter block, and dye was iontophoretically injected into Purkinje cell dendrites located in the molecular layer, using 0.4 Hz current pulses of –15 to –40 nA. The injections were continued for 10–15 min, until all dendritic branches of a Purkinje cell were completely filled and fluoresced brightly (Fig. 1A). A total number of 112 different cells were filled in the four different genotypes. Between 18 and 23 Purkinje cells were injected per genotype.

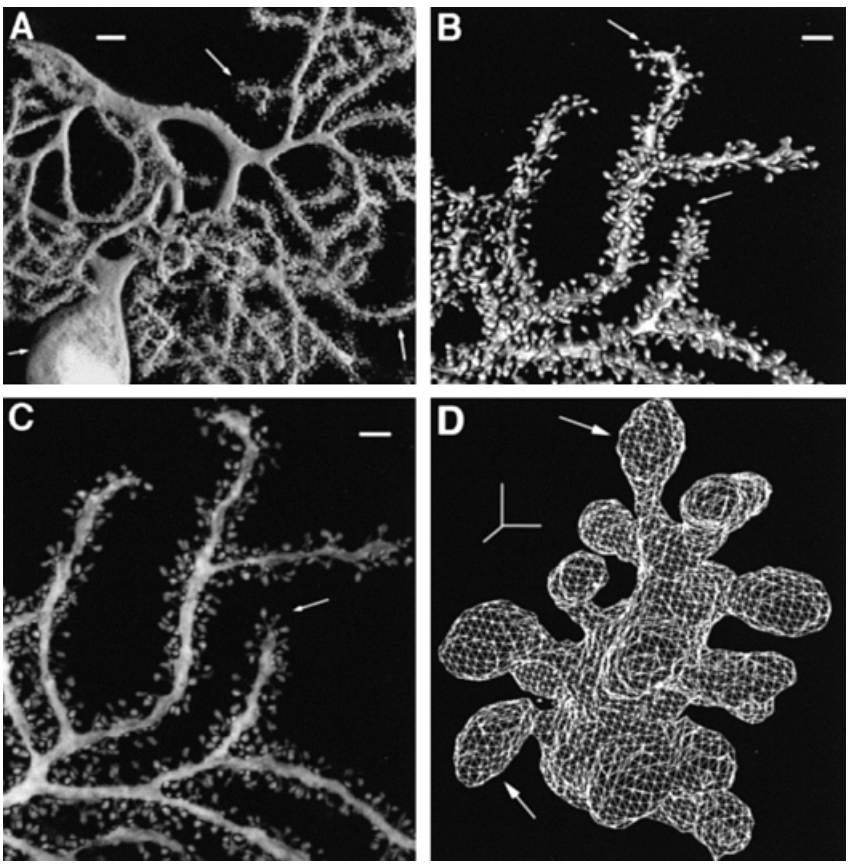

FIG. 1. Demonstration of the methodological approach. (A) A shadow projection of a Lucifer Yellow injected wild-type Purkinje cell with perikaryon (small arrow) and first-, second- and third-order dendrites (large arrows) which are studded with a multitude of spines. Note that single-cell injection provides an excellent signal to background ratio, important for accurate reconstructions near the optical resolution. Scale bar, 4 µm. (B) A reconstruction of dendritic fragments with their spines in wild-type mice based on isosurface-models. Arrows point to terminal dendrites studded with spines. Scale bar, 2.5 µm. (C) A frontal projection of the same dendritic fragments in wild-type mice. Note the loss of volume information. (D) A wire frame-model of a dendritic fragment with its spines in a virtual 3-D space, in which they can be turned arbitrarily around an axis for analysis. Additional spines could be detected which were normally obscured by the dendritic shaft. Arrows point to spine heads reconstructed by multiple polygons based on a matching cube algorithm. 3-D cursor, 0.5 µm.

Confocal laser scanning microscopy

Tissue containing dye-injected Purkinje cells was mounted in Slow Fade™ (Molecular Probes, Eugene, OR), coverslipped on spacers and scanned with an MRC-1200 BioRad krypton/argon CLSM (BioRad, Glattbrugg, Switzerland) with a software zoom between 1.5 and 4. Images were collected using a single channel on a blue filter set and at an excitation wavelength of 488 nm. Specimens were analysed using a 100 × (Nikon Apochromat) oil-immersion objective lens, with a numerical aperture (NA) of 1.4. The pinhole aperture was kept within the range 1.4–1.8. Photo-counting mode was used to enhance image collection. Z-series were taken at intervals of 0.1, 0.15 or 0.2 µm. The laser power was varied between 10 and 30% according to the specimen. Slow speed scanning was employed. All images of a single optical plane were Kalman-filtered by a factor of 7. The image stack was then saved on a magneto-optical disk (Cope) in the BioRad file format.

An obvious concern is the measurement of minute structures like spine heads and necks near the resolution limits of the confocal microscope. The specifications of our particular optics, according to the Rayleigh criteria, yield a theoretical lateral resolution of d_{min} of 0.21 µm (Inoué, 1995). However, it has been shown that with the use of confocal microscopy in a small field of view within the confocal plane, this theoretical limit can be increased by a factor of two (Wilson & Sheppard, 1984), thus producing an effective lateral resolution in the range of 0.1 µm. The axial resolution (measured along the optical axis of the microscope, i.e. perpendicular to the plane of focus) is given by $z_{min} = 2\ l_0 e/(NA)^2$, where l_0 is the wavelength of light, e is the refractive index of the object medium and NA the numerical aperture. The ratio of axial-to-lateral resolution is > 1 and inversely proportional to the NA of the objective. To determine the reliability of our measurements, fluorescent-labelled latex beads with diameters of 0.1 µm were reproducibly measured and distinguished from one another. In order to make a reliable reconstruction for the rendering of the image, we used a sampling frequency matched to the optical resolution with regard to Nyquist's theorem, which states that sampling frequency must be at least $2f$ (f = frequency) to sample a sinus wave. In reality, perfect reconstruction of the original signal from the sampled data requires a low-pass filter which was not available; therefore we usually used for nonperiodic objects $2.3 \times f$ as a minimum practical sampling rate. The most practical solution is then simply to adjust the zoom to match the Nyquist requirement.

Image analysis, measurements and statistics

From the image stacks, isosurface polygon models of selected terminal branchlets ($n = 25$ for each genotype) were computed. These allowed a detailed quantitative spine study, i.e. measurement of spine length, spine volume and spine surface areas. This analysis was performed with a Silicon Graphics SceneViewer and CosmoWorld using an Imaris DepthView program (Bitplane AG, Zurich) on a Silicon Graphics workstation (Octane) under Irix 6.4 and X-Window. In the first step, the voxel-space was analysed by 'slicing' through the image stack and counting the spine density on the individual 2D-planes, and focusing on regions of interest accordingly. In a second, improved approach, 3-D isosurface wire frame models were used and analysed. Image-filtering routines, such as γ-contrast stretch and median- and gaussian-filtering were not used, to prevent unwanted additional biases. In total, 100 dendritic fragments of terminal branchlets, each with numerous spines, were analysed and served as a database for computing and reconstructing 100 3-D isosurface wire-frame models. For each of the four genotypes (wild-type, $PV^{-/-}$, $CB^{-/-}$, $PV^{-/-}CB^{-/-}$ double knock-out) 25 terminal dendritic fragments were chosen randomly and the following were quantified.

Density of spines

This was expressed as the ratio of spines per length of dendrite. (i) Counts were made using 2-D optical sections through the tissue and subsequent manual slicing through the magnified region of interest. This method has its inherent drawbacks as spines which project vertically from the near and far sides of the dendrite are often overlooked as they are almost totally obscured by the brighter dendritic shaft. (ii) Counts were performed on 3-D isosurface models of the dendritic fragment. One of the best ways to visualize a 3-D structure is to display a series of projections along a fixed rotational axis. We therefore used a 3-D rendering method based on the marching cube algorithm to generate a list of polygons which represent accurately the surface of the dendrites and spines (Cline *et al*., 1988). By turning these models arbitrarily on the screen, it was possible to detect a considerable number of additional spines. Furthermore, it was easier and more accurate to categorize spine morphology because of their enhanced appearance.

Spine length

For each genotype, 250 individual spines were measured. The length of the spines was defined as the distance between the dendritic stem surface and the tip of the spine.

Spine volumes and spine surfaces

For each genotype, 50 characteristic spines were selected randomly and reconstructed by isosurface rendering. Spine volume and spine surface were measured with the Imaris depth view analyser and marching cube algorithm.

Topographic spine distribution as an indicator for second-order properties of spine layout in terms of clustering or ordering along dendrites

This is a characteristic that is not revealed by mean longitudinal density. In each dendritic fragment, 10 consecutive interspine distances were measured along the dendrite ($n = 250$ for each genotype). The distribution pattern of this interspinal data set, {di}, allowed an assessment of second-order properties where the degree of clustered distribution is reflected by an inhomogeneous and asymmetric histogram.

Classification of spine subtypes

Spines were classified in two populations, i.e. archetypical spines with a significant, clearly distinguishable stem and club-shaped head which represent the majority of spines (group A) and stubby spines, without any significant stem, their head protruding directly from the dendritic stem (group B). The percentage of type A and B spines in the different genotypes was calculated.

Density, length, volume and surface area were subjected to statistical analysis by a one way ANOVA Kruskal–Wallis-Test and a nonparameterized Mann–Whitney *U*-test.

Results

On a low magnification (10 ×) no differences in Purkinje cell structure between the different genotypes were observed. The size and localization of their perikarya was normal, the thickness of the strata moleculare and granulare appeared to be the same in all genotypes. More importantly, the dendritic tree patterns appeared similar.

Terminal branchlets, or terminal dendrites, were represented mainly by tertiary or successive end-branches (Fig. 1) rising towards the surface or curling downwards towards the granular layer in a random pattern of distribution. In all genotypes, these terminal branchlets were covered with numerous spines (e.g. Fig. 1) which projected from all sides, similar to the bristles on a bottle brush. Their localization was to a certain degree bipolar (see below, Fig. 3D, 3E and 3I), thus reflecting the unique anatomical structure of the dendritic tree, which spreads out in a vertical plane at right angles to the longitudinal axis of the cerebellar folium. Each terminal branchlet was characterized by its length, dendritic mean diameter and orientation in space. The dendritic mean diameter was calculated by the measurement of three randomly located regions within the same fragment. In order to minimize a possible counting bias in 3-D space, mainly dendritic fragments which appeared almost parallel to the specimen surface were chosen. However, their curvature perpendicular to this plane was not known; thus, true dendritic length may be underestimated. Considering that the curvature in the plane of view as well as that in the invisible perpendicular plane are similar, one may assess the degree of departure of the visible dendrite from a straight line and then use the same coefficient to correct the curvature (Rusakov & Stewart, 1995). Such an equivalence is justified as the visible side of a dendritic fragment is purely random. Using this approach for the fragments examined, there was an underestimation in length of 3% of the recorded values, where small dendritic fragments constituted a straight line.

Spine lengths

Measurements of spine lengths in wild-type mice (Figs 2P, 2Q, 2T, 3B and 3F) gave mean (± SD) values of 0.87 ± 0.21 µm, whereas spines of PV-deficient mice (Figs 2M, 2O, 3C, 3G and 3H) were 0.92 ± 021 µm in length. On average, longer spines were found in $CB^{-/-}$ mice (Figs 2F, 2G, 2H, 3D, 3I and 3J; mean length of 1.47 ± 0.39 µm). The longest spines were observed in the $CB^{-/-}PV^{-/-}$ double knock-out mice (Figs 2A, 2E, 3A and 3E; 2.21 ± 0.59 µm). In general, the longer the spines, the slimmer their necks appeared (Fig. 3E). These measurements were restricted primarily to type A spines which form the majority. The presence of significant differences between the four genotypes of mice is further corroborated by a nonparametric Kruskal–Wallis ANOVA test, also known as the *H*-test (Clauss *et al*., 1995) which showed a *P*-value and a tied-*P*-value < 0.001. The quantitative aspects of the spine length distribution are shown in Fig. 4A.

Spine volumes

Measurements of spine volumes in wild-type mice (Figs 2P, 3B and 3F) gave a value of 0.27 ± 0.12 µm^3 and spines of $PV^{-/-}$ mice (Figs 2L, 3C, 3G and 3H) were similar (0.26 ± 0.11 µm^3). On

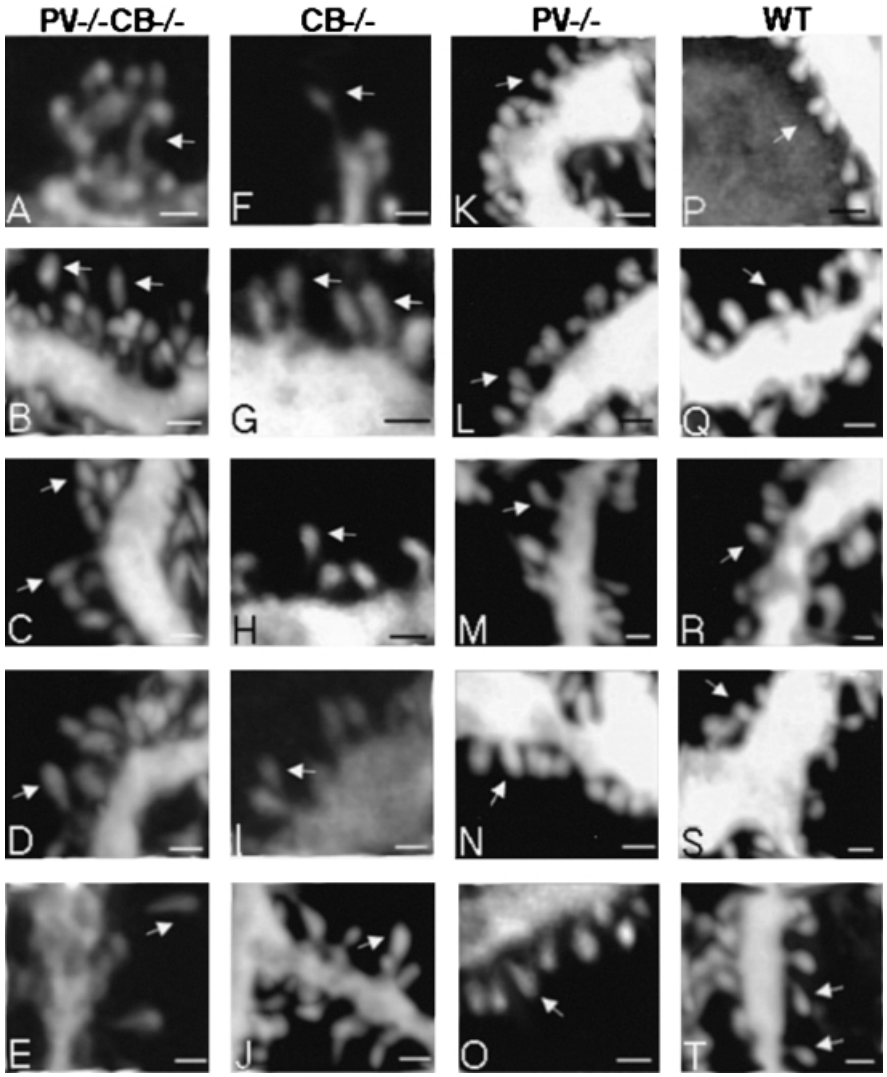

FIG. 2. Dendritic fragments studded with spines of different genotypes. (A–E) $PV^{-/-}CB^{-/-}$ double knock-out mice. (F–J) $CB^{-/-}$ mice. (K–O) $PV^{-/-}$ mice. (P–T) Wild-type animals. Note the more clustered distribution in (A–D), longer spines (arrows in A–E) and greater spine heads in the double knock-out mice. On the other hand, the distribution-pattern in wild-type mice is rather homogeneous (P, Q and T), their spines are smaller (P, S and T) and stubby spines appear more often. The $PV^{-/-}$ mice (K–O) also show small spines, their distribution is rather homogeneous. $CB^{-/-}$ animals show larger spines (F, G, H and J), increased spine volumes and the beginning of a clustered distribution (G and J). Scale bar, 1 µm.

average, greater volumes were observed in $CB^{-/-}$ mice (Figs 2G, 3I and 3J; mean volume of 0.43 ± 0.14 μm^3). The greatest volumes, almost double the size compared with wild-type animals, were observed in the $CB^{-/-}PV^{-/-}$ double knock-out mice (Figs 2B, 2D, 3A and 3E; 0.58 ± 0.16 μm^3). In general, if spines were longer, not only did their necks appear slimmer but also their heads increased in size. Furthermore, their shape changed from sphere-like to more a drop-like appearance (e.g. Figure 2P vs. 2D or Fig. 3B vs. 3A). A nonparametric Kruskal–Wallis ANOVA test showed again a *P*-value and a tied-*P*-value < 0.001, indicating highly significant differences between the different genotypes (Fig. 4B).

Spine surfaces

Spine volumes were found to be different between genotypes (Fig. 4B); similarly, the spine surface areas are different. Because there is also an important difference in shape from spherical to drop-shaped, there is no direct correlation between surface and volume. Measurements of spine surfaces in wild-type mice (Figs 2P, 2S and 3F) yielded values of 4.5 ± 1.5 μm^2, whereas spine surfaces of $PV^{-/-}$ mice (Figs 2M, 3C, 3G and 3H) showed a slight decrease in surface area (3.2 ± 0.7 μm^2). On the other hand, the mean surface area in $CB^{-/-}$ mice was 4.6 ± 1.3 μm^2 which is quite similar to that of the wild-type mice (Figs 2F, 2H and 3D). The largest surfaces areas were found in the $CB^{-/-}PV^{-/-}$ double knock-out mice (Figs 2A, 2C, 2D and 3E; 11.1 ± 3.6 μm^2). A nonparametric Kruskal–Wallis ANOVA test showed a *P*-value and tied-*P*-value both < 0.001 (Fig. 4C).

Spine density

In conventional 2-D counting, the archetypical spines (type A) of wild-type mice expressed 3.15 ± 0.61 spines/μm (Figs 2P, 2Q and 3B). The density in $PV^{-/-}$ mice was 3.12 ± 0.60 spines/μm (Figs 2N, 2O and 3G), but this was increased in $CB^{-/-}$ mice to 3.37 ± 0.62 spines/μm (Figs 2J, 3D and 3I). In the $CB^{-/-}PV^{-/-}$ double knock-out animals the mean density was further increased to 4.38 ± 1.56 spines/μm (Fig. 2B–2D). Applying the 3-D rendering method (Fig. 1B and 1D), the density in wild-type mice increased to 3.41 ± 0.62 spines/μm, to 3.36 ± 0.70 spines/μm in $PV^{-/-}$, to 3.82 ± 0.73 spines/μm in $CB^{-/-}$and to 5.12 ± 1.86 spines/μm in $CB^{-/-}PV^{-/-}$ double knock-out mice. Compared with the 2-D approach, the values obtained from 3-D methods were elevated in all three genotypes; i.e. these increases were $7.4 \pm 2.9\%$ in wild-type, $6.6 \pm 3.6\%$ in $PV^{-/-}$ mice, $13.3 \pm 3.0\%$ in $CB^{-/-}$ mice and $14.0 \pm 3.6\%$ in $CB^{-/-}PV^{-/-}$ double knock-out mice (for method differences see Fig. 5). As the diameters of dendrites within the different genotypes are not exactly the same, i.e. 0.90 ± 0.22 μm for wild-type animals, 0.91 ± 0.24 μm for $PV^{-/-}$ animals, 1.07 ± 0.23 μm for $CB^{-/-}$ animals and 1.23 ± 0.34 μm for $CB^{-/-}PV^{-/-}$ animals (Fig. 4F), the increase in the number of spines is not equal for all genotypes, as broader dendritic stems tend to hide spines more easily than thinner ones. Figure 4D shows the density-

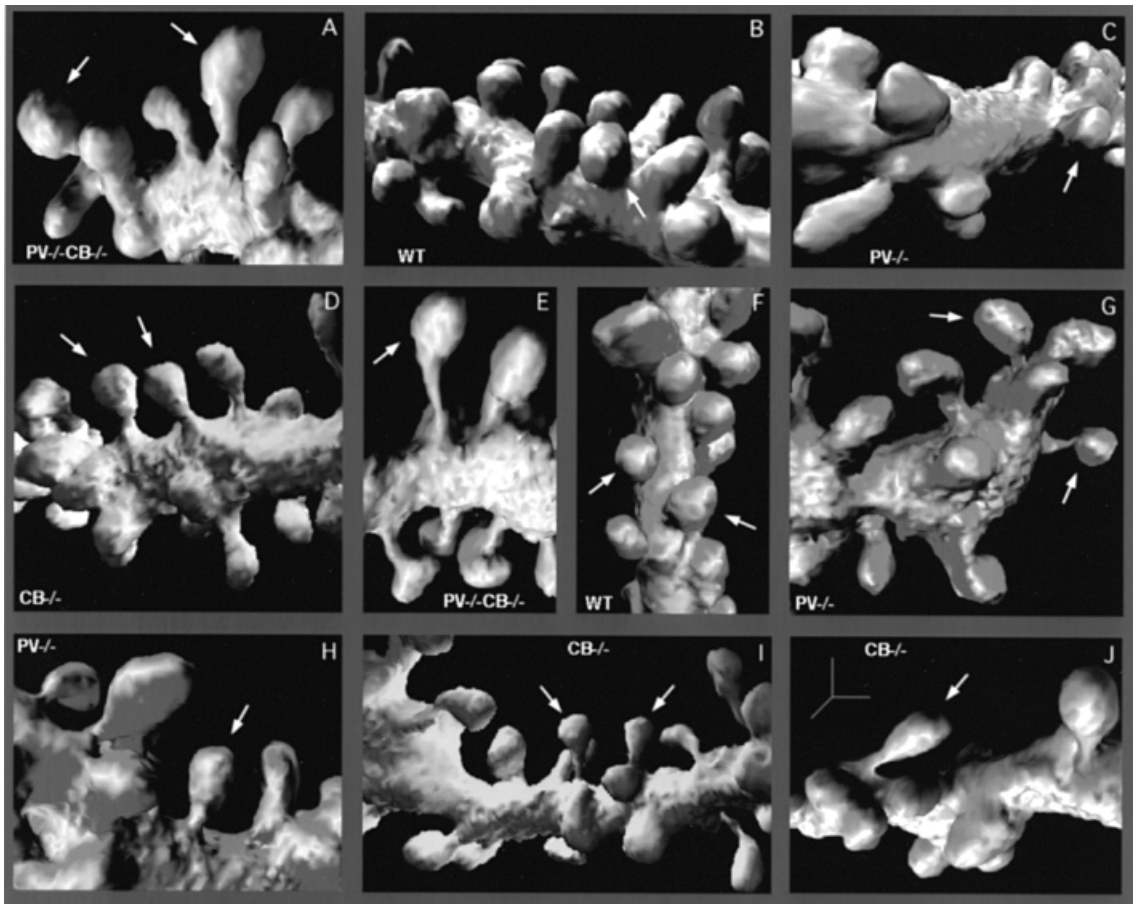

FIG. 3. Enlightened 3-D models of dendritic fragments in a virtual space. (A and E) $PV^{-/-}CB^{-/-}$ double knock-out mice. (D, I and J) $CB^{-/-}$ mice. (C, G and H) $PV^{-/-}$ mice. (B and F) Wild-type mice. Note longer spines (arrow in E) and more pronounced spine heads (arrows in A) in the double knock-out animals. Typical stubby formed spines of wild-type mice with no significant stem are shown in parts B and F (arrows). $PV^{-/-}$ mice also show small spines (arrow in H) and stubby spines (arrow in C). In $CB^{-/-}$ mice, spines are longer (arrows in D, I and J) and are more clustered (I). Also note the general bimodal appearance of spines in space (e.g. in D, G and I). 3-D scale (J) corresponds to 0.5 μm for all images, but due to true 3-D projections, distortions must be taken into account.

distribution for each genotype, subdivided by the 2-D and 3-D approach, respectively. Tenth, 25th, 50th, 75th and 90th distribution percentiles are indicated, as well as those single values lying below the 10th or above the 90th percentiles. The middle bar represents the geometric mean.

Stubby spines

Conglomerates of stubby spines were present in wild-type animals (Figs 2P, 3B and 3F). A homogeneous distribution was observed along the dendritic stem (Figs 2P, 2T and 3F). The proportion of these stubby spines in relation to the whole spine number was 15.9 ± 2.7% in wild-type mice, 13.3 ± 3.5% in $PV^{-/-}$ mice, 13.0 ± 2.0% in $CB^{-/-}$ mice and 10.0 ± 3.5% in the double knock-out mice. Thus, the PV-CB-deficient mice, which were characterized by the longest spines (e.g. Figs 2A, 2B, 2E, 3A and 3E), contain the smallest percentage of stubby spines (Fig. 2B–2D). The relative abundance of type B spines in the different genotypes is shown in Fig. 4E. Furthermore, with a decrease of stubby spines, the whole spatial distribution was found to be more inhomogeneously spread along the dendrite and very clustered in double knock-out animals (Figs 2A, 2C, 2D and 3A) and also in $CB^{-/-}$ mice (Figs 2G, 2J and 3H).

Spine topology

Distribution patterns of the interspine dataset are shown for each genotype (Fig. 6). The $CB^{-/-}PV^{-/-}$ mice showed a strikingly different distribution pattern compared with the other three genotypes. First, interspine distances extend over a much broader range (maximum value 4.8 µm, minimum value 0.2 µm). Second, there is an accumulation in the low range, with a greater number of interspine distances below 1 µm. The distribution pattern is unimodal and slanting, reflecting a c-distribution, where a calculated mean value was 1.37 ± 0.89 µm. This reflects a more clustered and inhomoge-

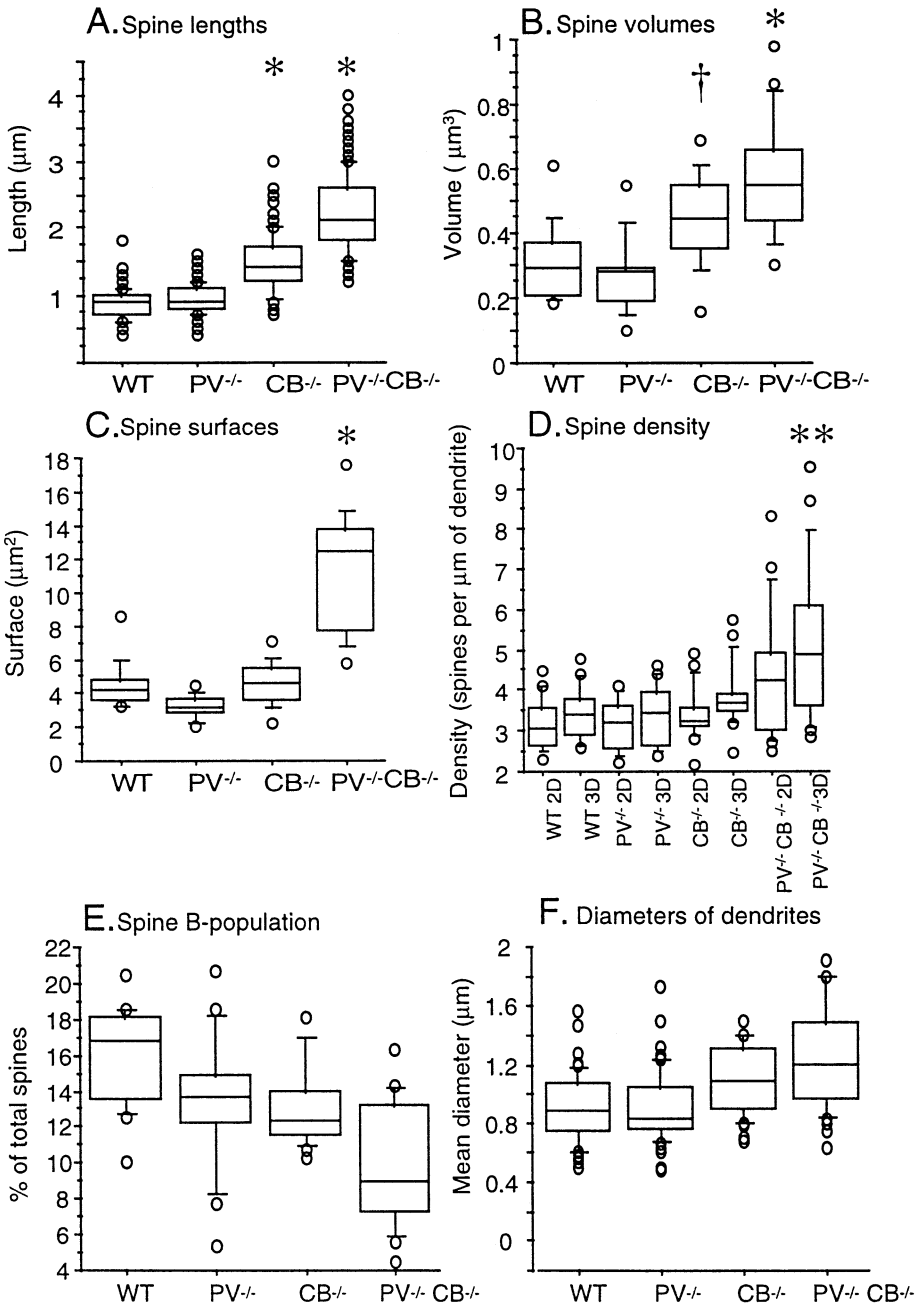

FIG. 4. Diagrams of density-distributions of the most important spine characteristics calculated for each genotype. The horizontal lines indicate 10th, 25th, 50th, 75th and 90th distribution percentiles. Single values lying below the 10th or above the 90th percentiles are shown as small circles. (A) Spine lengths, where $PV^{-/-}CB^{-/-}$ double knock-out mice show the longest. * Statistically significant vs. wild-type ($P < 0.0001$; Mann–Whitney *U*-test; $n = 250$). (B) Spine volumes are increased in double knock-out mice, and the values for $CB^{-/-}$ mice are intermediate between $PV^{-/-}CB^{-/-}$ double knock-out and either wild-type (WT) or $PV^{-/-}$. *$P < 0.0001$ and †$P < 0.002$, compared with WT ($n = 50$). (C) Spine surfaces are increased mainly in the $PV^{-/-}CB^{-/-}$ double knock-out mice ($P < 0.0001$, $PV^{-/-}CB^{-/-}$ vs. WT; $n = 50$). (D) Spine density is considerably higher in the $PV^{-/-}CB^{-/-}$ double knock-out animals determined by 2-D or 3-D counting. **$P < 0.001$, compared with WT ($n = 250$). (E) The percentage of stubby spines (B population) is relatively small in all animals, but lowest in the double knock-out mice ($n = 25$). (F) Differences between the diameters of dendrites ($n = 25$).

neous spine distribution in the double-knock-out mice (Fig. 2A, 2D and 2E). In contrast, the topology in wild-type and $PV^{-/-}$ mice is similar and reflects a normal distribution pattern (Fig. 3H and 3I). Also, the area under the curve fits well to a hypothesized normal distribution, a symmetry pattern of the interspine distances is clearly evident (also see Fig. 2P, 2T, 2L and 2N). Mean values are $0.91 \pm 0.22\,\mu m$ for wild-type mice and $0.99 \pm 0.26\,\mu m$ for $PV^{-/-}$ animals, respectively. Note that also the standard deviation is much smaller in wild-type mice compared with the double knock-out animals. Furthermore, maximum values never exceeded $2\,\mu m$ (wild-type, $1.6\,\mu m$ and PV knock-out $1.8\,\mu m$). The $CB^{-/-}$ genotype lies between wild-type and double-knock-out with respect to topology; its distribution pattern still fits a normal distribution well (Fig. 6). On the other hand, a broader range is evident and the maximum increases to $3.5\,\mu m$, whereas the calculated mean value was $1.22 \pm 0.41\,\mu m$. These findings for the $CB^{-/-}$ genotype reflect a more inhomogeneous distribution than in $PV^{-/-}$ or wild-type mice, but clustering of spines is not yet clearly evident as in the $CB^{-/-}PV^{-/-}$ double knock-out animals (Figs 2G, 2I, 2J and 3I).

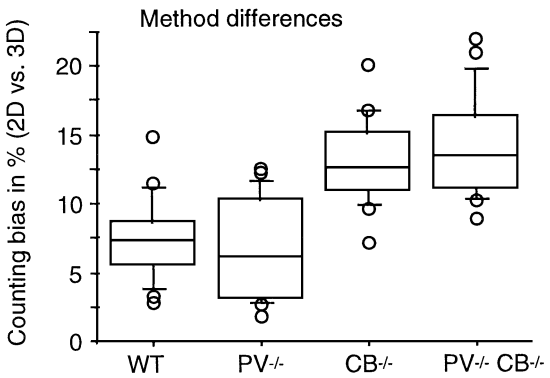

FIG. 5. Method differences with respect to the 2-D or 3-D counting approach, respectively ($n = 25$). The 3-D method allows the detection of spines which project vertically (in the Z-axis), as explained in Material and Methods. The error in the 2-D counting method increases with an increased diameter of the dendrite, since more spines will be obscured by the intense fluorescence of the dendritic shaft. The larger counting bias in the density of spines in $CB^{-/-}$ and $PV^{-/-}CB^{-/-}$ mice compared with WT or $PV^{-/-}$ spines is correlated with the increase in the diameters of the dendrites in $CB^{-/-}$ and $PV^{-/-}CB^{-/-}$ mice (see Fig. 4F).

Discussion

Spines

Spines, first described by Ramòn y Cajal (1891) in light microscopic studies of Golgi-stained tissue are abundant in Purkinje cells '…for in no other cells are they so short, so stout, or so abundant…..' There are numerous physiological hypotheses of the function of the dendritic spines, and recent technical advances like CLSM and direct visualization of calcium dynamics are now permitting the experimental testing of some of these theoretical concepts. Each Purkinje cell is studded with up to 200 000 spines, each one carrying a single excitatory synapse from a parallel fibre (Braitenberg & Atwood, 1958). Their shape varies widely (see also Figs 2 and 3), ranging from short and stubby through the archetypical 'mushroom-shaped', to long and thin (Jones & Powell, 1969). This classification remains somewhat arbitrary; the simplified division into two main groups (spines with a significant neck and spines without neck, respectively) seems to be the most reliable. In the cerebellum, the exact morphology of spines was first reported by Harris & Stevens (1988) by means of 3-D reconstructions of serial electron micrographic sections.

Both the absolute number as well as the shape of spines can change dramatically, with a number of external variables. Morphological changes during development and ageing have been reported (Feldman & Peters, 1979; Harris *et al.*, 1992). Further studies dealt with the number and distribution of dendritic spines (Feldman & Peters, 1979; Rusakov, 1993), their morphological changes in the learning process

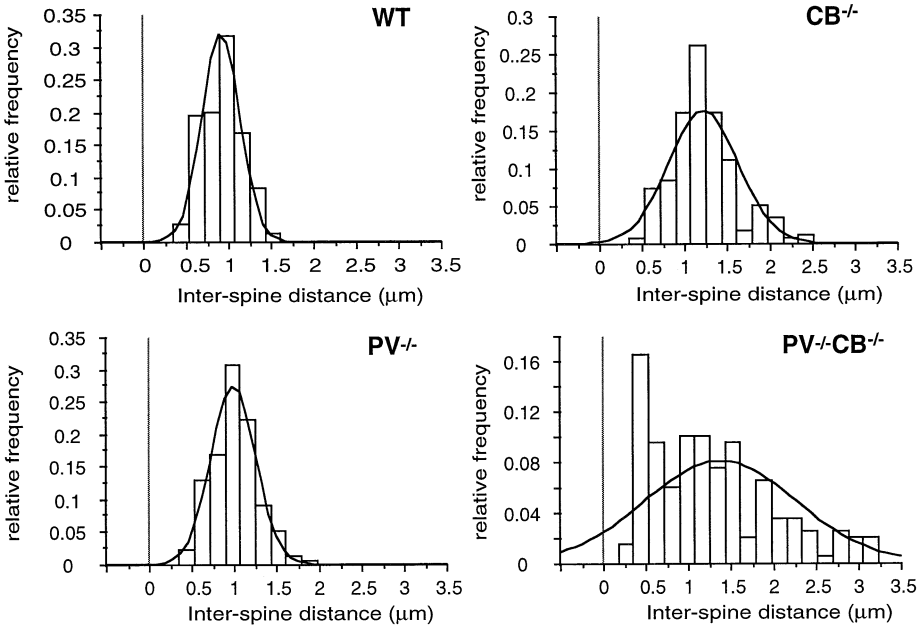

FIG. 6. Interspine distances are shown by histograms according to their relative frequency. These patterns allow an assessment of second-order properties like clustering along the dendrite. In the double knock-out mice a clustered distribution is most pronounced with an accumulation of short distances below 1 μm, and furthermore an increase in long distances (for explanation see text; $n = 250$).

and long-term potentiation (Berard *et al.*, 1981; Greenough & Chang, 1985), under experimental conditions (Rausch & Scheich, 1982; McKinney *et al.*, 1999), and in pathological states (Ferrer, 1988; Gähwiler *et al.*, 1997). Some of the reported changes include larger spine heads, changes in the shape of the spine stem and an increase in the number of shaft synapses. It is not yet known what role these changes in spine shape play in the increase of synaptic efficacy.

The two EF-hand type Ca^{2+}-binding proteins CB and PV are highly expressed in Purkinje cells and the large Ca^{2+}-binding ratio of these cells is related to the presence of these two Ca^{2+}-buffer proteins (Fierro & Llano, 1996). To address the significance of CB and PV in Purkinje cells, knock-out mice lacking either one or both of the two proteins were produced. We hypothesized that altered Ca^{2+} homeostasis in spines might alter their morphology. Spine parameters investigated in $PV^{-/-}$ mice were similar to control mice, while small, but significant changes (most notably spine length) were observed in $CB^{-/-}$ animals, suggesting that the lack of CB affects spine morphology more than the absence of PV. The main finding is that in the $PV^{-/-}CB^{-/-}$ double knock-out animals, spine necks are in general more slender, spines are longer and their volumes are almost doubled.

Technical considerations

In our 3-D graphics approach, the surface of the desired structure is approximated by a series of polygons, which form a wire frame model (Fig. 1D). The model is then displayed by selecting a viewing angle in the data space and projecting all the polygons onto a plane that is perpendicular to the viewing direction (all models in Fig. 3). Although rendering algorithms are well-developed, it can be difficult to generate a series of polygons that accurately represents the surface of the structure. In conjunction with the Imaris-modelling system (bitplane) a marching cube algorithm was used (Cline *et al.*, 1988), which defines the 3-D structure by a single threshold value throughout the data set. In the present study, the grey-level histograms of all images had two apparent peaks which correspond to two groups of pixels, i.e. dendrite with spines and the background. In our case, the apparent presence of the bottom of the valley between the histogram peaks provides a mathematically natural threshold for object vs. background separation (Li & Lee, 1993), which was used as the threshold between the two groups for the marching cube algorithm. Furthermore, the brightness scale of the captured images was normalized using a 'linear contrast stretch' to inhibit a shifting of the histogram grey levels towards either darker or brighter values.

Estimation of the true spine density

The ratio between visible and true numbers of spines observed via light/confocal microscopy depends on their dimension, shape, and spatial layout, in addition to the width of the dendritic stem. Thus, estimation of the true spine density along dendrites is an important issue in neuromorphology, and a number of stereological correction factors have been proposed in the literature (Feldman & Peters, 1979; Rusakov, 1993). The methods used in this study reduce the stereological bias in spine counts incorporating dimension, shape and spatial orientation. Counting spines in the turnable 3-D wire frame models resulted in an increase of spine density of 7–14% (Figs 4D and 5) in different genotypes and reduced the bias considerably. Additional spines were detected due to more accurate visualization of spines which were either hidden behind the opaque, impregnated dendritic shaft or lay in its shadow and were consequently not observed. The models allowed a qualitative approach to the data set and enabled a distinction between shape and appearance of spines not possible with other powerful methods like the disector (Sterio, 1984) or line skeleton binary algorithms (Bookstein, 1979) because of an inherent loss of volume-information. Important second-order properties, like ordering and clustering of spines along the dendrite (e.g. Figure 2B and 2I) could also be observed, which would be very difficult to appreciate using electron microscopy.

Comparison with other studies

In our study, mean spine density varied between 3.1 and 5.1 spines/μm of dendrite, depending on the genotype studied (Fig. 4D). Maxima and minima were between 2.6 and 4.8 spines/μm of dendrite in wild-type animals. Harris & Stevens (1988) found 11–14 spines/μm of dendrite by serial section electron microscopy (SSEM) of rat Purkinje cells, while in older papers, values between 1 and 4.5 spines/μm were reported (Fox *et al.*, 1964; Palkovits *et al.*, 1971; Smolyaninov, 1971; Palay & Chan-Palay, 1974). The differences may be partly attributed to species differences (human, monkey, cat, rat, mouse) and also methodological differences. A disadvantage of EM is the thorough fixation required, which unlike the gentle procedures used in this study, result in increased tissue shrinkage. On the other hand, there is a better spatial resolution in SSEM compared with light microscopy where the optical resolution is around 0.1 μm. Furthermore, dye concentration in the smallest spines has been shown previously to be less than approximately 1% of that of dendrites (Svoboda *et al.*, 1996), thus excluding their distinction from the background fluorescence derived from light scattering in the tissue. In the same study, the spine density on rat hippocampal CA1 pyramidal neurons determined by two-photon laser scanning microscopy was approximately twofold lower (1.3 vs. 2.5) compared with determination by SSEM (Harris & Stevens, 1989). Less than half the density of spines observed by SSEM were also reported by Kirov & Harris (1999) using confocal microscopy. Thus, very thin spines are not detected and closely spaced clusters of thin spines, as reported by Harris & Stevens (1988), will be recognized as one large spine by CLSM leading to the apparent smaller density. The spine length (0.87 ± 0.21 μm) in wild-type mice was similar to that reported in rat (1.22 ± 0.30 μm). Also in this case curvature of the spines out of the plane of focus leads to an underestimation of the spine length by CLSM. On the other hand, the spine volume (0.27 ± 0.12 μm^3) was larger than that found for rat spines (0.12 ± 0.02 μm^3) by SSEM. Besides the same considerations as for the spine density (loss of small structures or 'integration' of closely spaced spines into a single one), the relative 'fuzziness' of fluorescence leads to an increased 'apparent' size of spines. Nevertheless, the systematic errors inherent in CLSM are the same for all the genotypes tested. The spine density was considerably higher in the $PV^{-/-}CB^{-/-}$ double knock-out animals, $CB^{-/-}$ mice have a slightly increased density, whereas between wild-type and $PV^{-/-}$ mice no significant differences were observed.

Biological implications

In Purkinje cells, synaptically evoked increases of $[Ca^{2+}]_i$ are, in part, mediated by Ca^{2+} influx through AMPA-type glutamate receptors and voltage-activated calcium channels (Llano *et al.*, 1991; Eilers *et al.*, 1995) and, on a slower time scale, by activation of metabotropic glutamate receptors (mGluR1) which results in inositol-1,4,5-trisphosphate (InsP3)-induced Ca^{2+} release (Finch & Augustine, 1998; Takechi *et al.*, 1998). These changes in intracellular Ca^{2+} appear to be restricted to spines or terminal spino-dendritic compartments (Denk *et al.*, 1995; Eilers *et al.*, 1995; Takechi *et al.*, 1998). There is now accumulating evidence for a reciprocal interplay between spine morphology and spine Ca^{2+}. Experimentally this was demonstrated in cultured hippocampal neurons by Volfovsky *et al.* (1999). They

observed that a short spine neck increases the magnitude of the Ca^{2+} response in the dendrite and speeds up the recovery in the spine head. Mobile Ca^{2+} buffers within spines are likely to affect both processes. Therefore, the changes in spine morphology, i.e. increase in spine length and volume, reported in this study may compensate for the loss of mobile Ca^{2+} buffers. Our results show that loss of CB, which in Purkinje cells appears to act as a fast Ca^{2+} buffer (Airaksinen *et al*., 1997), is more critical than the lack of PV. However, the biochemical properties and possibly the subcellular distribution of these proteins are not identical and this may contribute to the observed differences. On the other hand, there are recent reports which demonstrate a correlation between Ca^{2+} homeostasis and spine morphology. Release of Ca^{2+} from internal stores in cultured hippocampal neurons leads to an increase of spine length (Korkotian & Segal, 1999). Assuming that this also applies to Ca^{2+} derived from other sources and to Purkinje cell spines, this suggests a balanced interplay between spine morphology and spine Ca^{2+} which is optimized with respect to yet unknown functional characteristics of individual synapses. Mobile Ca^{2+} buffers would shift this balance towards shorter and smaller spines without losing the Ca^{2+} regulation otherwise possible only in larger spines.

This interplay of spine morphology and spine Ca^{2+} may also serve to protect the parent dendrite from a rise of $[Ca^{2+}]_i$ to toxic levels (Segal, 1995). Thus, synaptic activity, which can raise $[Ca^{2+}]_i$ in a single spine to a high level, will not harm the parent dendrite provided spine morphology is adequately adapted. This is particularly important in distal dendrites, the diameter of which is often smaller than that of the corresponding spines. Together with Ca^{2+} extrusion mechanisms 'soluble transient Ca^{2+} stores' like PV and CB can limit Ca^{2+} accumulation and thereby protect spines against excessive Ca^{2+} levels. Increasing the spine volume would again provide a straightforward mechanism of compensation. Further studies are required to determine whether Ca^{2+}-dependent degradation/regression of spines is enhanced in these mutant mice.

The changes in spine morphology discussed above together with the observed changed topology of stubby spines may be important determinants of the peculiar ataxia found in CB null mutants (Airaksinen *et al*., 1997) and in $PV^{-/-}CB^{-/-}$ double knock-out mice (B. Schwaller, unpublished). Because stubby spines are thought to be the sites of climbing fibre synapses (Palay & Chan-Palay, 1974) postsynaptic sites of both major inputs (parallel and climbing fibres) to the principal neuron of the cerebellar cortex have undergone subtle morphological changes in these mutants. Consequences of these changes on cerebellar learning and its putative electrophysiological correlate, long-term depression, await analysis.

Acknowledgements

We thank Drs Pavel Belichenko and Daniela Vogt-Weisenhorn for technical advice and Dr Peter Eggli for the help with preliminary experiments with the CLSM. We are grateful to Drs Merdol Ibrahim, Anne McKinney, Pierre-Alain Menoud and Thomas Pauls for constructive discussion. In addition, this work has profited from the helpful and detailed comments of a reviewer. The project was supported by the Swiss National Science Foundation (grant no. 3100-047291.96 to M.R.C.), by the DFG (grant no. ME1121/3 to M.M.) and Novartis.

Abbreviations

AMPA, α-amino-3-hydroxy-5-methyl-4-isoxazolepropionic acid; 2-D, two-dimensional; 3-D, three-dimensional; CB, calbindin D-28 k; CLSM, confocal laser scanning microscopy; mGluR1, metabotropic glutamate-responsive receptor type 1; NA, numerical aperture; PB, phosphate buffer; SSEM, serial sections electron microscopy.

References

Airaksinen, M.S., Eilers, J., Garaschuk, O., Thoenen, H., Konnerth, A. & Meyer, M. (1997) Ataxia and altered dendritic calcium signaling in mice carrying a targeted null mutation of the calbindin D28k gene. *Proc. Natl Acad. Sci. USA*, **94**, 1488–1493.

Andressen, C., Blümcke, I. & Celio, M.R. (1993) Calcium-binding proteins: selective markers of nerve cells. *Cell Tissue Res.*, **271**, 171–208.

Andressen, C., Gotzos, V., Berchtold, M.W., Pauls, T.L., Schwaller, B., Fellay, B. & Celio, M.R. (1995) Changes in shape and motility of cells transfected with parvalbumin cDNA. *Exp. Cell Res.*, **219**, 420–426.

Belichenko, P.V. (1991) Development of an intracellular Lucifer Yellow method for studying neuronal structure in autopsies of the human brain. *Arch. Anat. Histol. Embryol.*, **101**, 81–84.

Berard, D.R., Burgess, J.W. & Coss, R.G. (1981) Plasticity of dendritic spine formation: a state-dependent stochastic process. *Int. J. Neurosci.*, **13**, 93–98.

Bookstein, F.L. (1979) The line skeleton. *Comp. Graph. Image Process.*, **11**, 123–137.

Braitenberg, V. & Atwood, R.P. (1958) Morphological observations in the cerebellar cortex. *J. Comp. Neurol.*, **109**, 1–34.

Buhl, E.H. & Schlote, W. (1987) Intracellular Lucifer Yellow staining and electron microscopy of neurons in slices of fixed epitumorous human cortical tissue. *Acta Neuropathol.*, **75**, 140–146.

Carafoli, E. (1987) Intracellular calcium homeostasis. *Annu. Rev. Biochem.*, **56**, 395–433.

Celio, M.R. (1990) Calbindin D-28k and parvalbumin in the rat nervous system. *Neuroscience*, **35**, 375–475.

Chard, P.S., Bleakman, D., Christakos, S., Fullmer, C.S. & Miller, R.J. (1993) Calcium buffering properties of calbindin D28k and parvalbumin in rat sensory neurones. *J. Physiol. (Lond.)*, **472**, 341–357.

Clauss, G., Finze, F.R. & Partzsch, L. (1995) *Der Vergleich von mehr als zwei Verteilungen auf der Grundlage unabhängiger Stichproben*. Harri Deutsch, Frankfurt am Main.

Cline, H.E., Lorensen, W.E., Ludke, S., Crawford, C.R. & Teeter, B.C. (1988) Two algorithms for the three-dimensional reconsruction of tomograms. *Med. Physics*, **15**, 320–327.

Denk, W., Sugimori, M. & Llinas, R. (1995) Two types of calcium response limited to single spines in cerebellar Purkinje cells. *Proc. Natl Acad. Sci. USA*, **92**, 8279–8282.

Eilers, J., Augustine, G.J. & Konnerth, A. (1995) Subthreshold synaptic Ca2+ signalling in fine dendrites and spines of cerebellar Purkinje neurons. *Nature*, **373**, 155–158.

Feldman, M.L. & Peters, A. (1979) A technique for estimating total spine numbers on Golgi-impregnated dendrites. *J. Comp. Neurol.*, **188**, 527–542.

Ferrer, I. (1988) Purkinje cells in degenerative disease. *Clin. Neuropathol.*, **7**, 22–28.

Fierro, L. & Llano, I. (1996) High endogenous calcium buffering in Purkinje cells from rat cerebellar slices. *J. Physiol. (Lond.)*, **496**, 617–625.

Finch, E.A. & Augustine, G.J. (1998) Local calcium signalling by inositol-1,4,5-trisphosphate in Purkinje cell dendrites. *Nature*, **396**, 753–756.

Fox, C.A., Siegesmund, K.A. & Dutta, C.R. (1964) The Purkinje cell dendritic branchlets and their relation with the parallel fibers. In: *Light and Electron Microscopic Observations.* Hoeber-Harper & Row, New York.

Gähwiler, H., Capogna, M., Debanne, D., McKinney, R.A. & Thompson, S.M. (1997) Organotypic slice cultures: a technique has come of age. *Trends Neurosci.*, **20**, 471–477.

Greenough, W.T. & Chang, F.L.F. (1985) Synaptic structural correlates of information storage in the mammalian nervous system. In Cotman, C.W. (ed.), *Synaptic Plasticity*. Guilford, New York, pp. 335–375.

Harris, K.M., Jensen, F.E. & Tsao, B.H. (1992) Three-dimensional structure of dendritic spines and synapses in rat hippocampus (CA1) at postnatal day 15 and adult ages: implications for the maturation of synaptic physiology and long-term potentiation. *J. Neurosci.*, **12**, 2685–2705.

Harris, K.M. & Stevens, J.K. (1988) Dendritic spines of rat cerebellar Purkinje cells: serial electron microscopy with reference to their biophysical characteristics. *J. Neurosci.*, **9**, 2982–2997.

Harris, K.M. & Stevens, J.K. (1989) Dendritic spines of CA1 pyramidal cells in the rat hippocampus: serial electron microscopy with reference to their biophysical characteristics. *J. Neurosci.*, **9**, 2982–2997.

Heizmann, C.W. (1984) Parvalbumin, an intracellular calcium-binding protein; distribution, properties and possible roles in mammalian cells. *Experientia*, **40**, 910–921.

Heizmann, C.W. & Braun, K. (1992) Changes in Ca2+-binding proteins in human neurodegenerative disorders. *Trends Neurosci.*, **15**, 259–264.

Hennings, H., Michael, D., Cheng, C., Steinert, P., Holbrook, K. & Yuspa,

S.H. (1980) Calcium regulation of growth and differentiation of epidermal cells in culture. *Cell*, **19**, 245–254.
Inoué, S. (1995) Foundations of confocal scanned imaging in light microscopy. In Pawley, J.B. (ed.), *Handbook of Biological Confocal Microscopy*. Plenum Press, New York, pp. 1–17.
Jones, E.G. & Powell, T.P.S. (1969) Morphological variations in the dendritic spines of neocortex. *J. Cell Sci.*, **6**, 509–529.
Kirov, S.A. & Harris, K.M. (1999) Dendrites are more spiny on mature hippocampal neurons when synapses are inactivated. *Nature Neurosci.*, **2**, 878–883.
Koch, C. & Zador, A. (1993) The function of dendritic spines: Devices subserving biochemichal rather than electrical compartmentalization. *J. Neurosci.*, **13**, 413–422.
Korkotian, E. & Segal, M. (1999) Release of calcium from stores alters the morphology of dendritic spines in cultured hippocampal neurons. *Proc. Natl Acad. Sci. USA*, **96**, 12068–12072.
Li, C.H. & Lee, C.K. (1993) Minimum cross entropy tresholding. *Pattern Recognit.*, **26**, 617–625.
Llano, I., Dreessen, J., Kano, M. & Konnerth, A. (1991) Intradendritic release of calcium induced by glutamate in cerebellar Purkinje cells. *Neuron*, **7**, 577–583.
Marks, P.W. & Maxfield, F.R. (1990) Transient increases in cytosolic free calcium appear to be required for the migration of adherent human neutrophils. *J. Cell Biol.*, **110**, 43–52.
McKinney, R.A., Capogna, M., Durr, R., Gahwiler, B.H. & Thompson, S.M. (1999) Miniature synaptic events maintain dendritic spines via AMPA receptor activation. *Nature Neurosci.*, **2**, 44–49.
Palay, P. & Chan-Palay, V. (1974). *The Cerebellum*. Springer, Berlin.
Palkovits, M., Magyar, P. & Szentagothai, J. (1971) Quantitative histological analysis of the cerebellar cortex in the cat. I. Number and arrangement in space of the Purkinje cells. *Brain Res.*, **32**, 1–13.
Ramon y Cajal, S. (1891) Histologie du système nerveux de l'homme et des vertebrés. Vol. 2. L. Azoulay transl. (1909–1911). Maloine, Paris, p. 155.
Rasmussen, C.D. & Means, A.R. (1989) Calmodulin, cell growth and gene expression. *Trends Neurosci.*, **12**, 433–438.
Rausch, G. & Scheich, H. (1982) Dendritic spine loss and enlargement during maturation of the speech control system in the mynah bird (Gracula religiosa). *Neurosci. Lett.*, **29**, 129–133.
Rusakov, D.A. (1993) Estimation of the size distribution of closed cell elements from analysis of their plane random sections. *Biometrics*, **49**, 141–149.
Rusakov, D.A. & Stewart, M.G. (1995) Quantification of dendritic spine populations using image analysis and a tilting disector. *J. Neurosci. Meth.*, **60**, 11–21.
Schwaller, B., Dick, J., Dhoot, G., Carroll, S., Vrbova, G., Nicotera, P., Pette, D., Wyss, A., Bluethmann, H., Hunziker, W. & Celio, M.R. (1999) Prolonged contraction-relaxation cycle of fast-twitch muscles in parvalbumin-knock-out mice. *Am. J. Physiol.*, **276**, (*Cell Physiol.*, **45**), C395–C403.
Segal, M. (1995) Dendritic spines for neuroprotection: a hypothesis. *Trends Neurosci.*, **18**, 468–471.
Smolyaninov, V.V. (1971) Some special features of organization of the cerebellar cortex. In Gelfand, I.M., Gurfinkel, V.S., Fomin, S.V. & Tsetlin, M.L. (eds), *Models of the Structural-Functional Organization of Certain Biological Systems*. MIT Press, Cambridge, pp. 250–423.
Sterio, D.C. (1984) The unbiased estimation of number and sizes of arbitrary particles using the disector. *J. Microscopy*, **134**, 127–136.
Svoboda, K., Tank, D.W. & Denk, W. (1996) Direct measurement of coupling between dendritic spines and shafts. *Science*, **272**, 716–719.
Takechi, H., Eilers, J. & Konnerth, A. (1998) A new class of synaptic response involving calcium release in dendritic spines. *Nature*, **396**, 757–760.
Volfovsky, N., Parnas, H., Segal, M. & Korkotian, E. (1999) Geometry of dendritic spines affects calcium dynamics in hippocampal neurons: theory and experiments. *J. Neurophysiol.*, **82**, 450–462.
Weruaga-Prieto, E., Eggli, P. & Celio, M.R. (1996) Topographic variations in rat brain oligodendrocyte morphology elucidated by injection of Lucifer Yellow in fixed tissue slices. *J. Neurocytol.*, **25**, 19–31.
Wilson, T. & Sheppard, C. (1984). *Theory and Practice of Scanning Optical Microscopy*. Academic Press, New York.
Yuste, R. & Denk, W. (1995) Dendritic spines as basic functional units of neuronal integration. *Nature*, **375**, 682–684.